Optical Properties of Pseudomorphic $Ge_{1-x-y}Si_xSn_y$ on Ge

Nalin S. Fernando,[1] Ryan Hickey,[2] John Hart,[2] Ramsey Hazbun,[2] Dainan Zhang,[2] James Kolodzey[2], Stefan Zollner[1]
[1]Department of Physics, New Mexico State University, MSC 3D, P.O. Box 30001, Las Cruces, NM 88003
[2] Department of Electrical and Computer Engineering, University of Delaware, Newark DE 19716

Introduction

- Ge is an indirect band gap material.
- Direct band gap → efficiency of the recombination process is high.
- Indirect band gap → requires an interaction with a phonon or defects. Very inefficient.

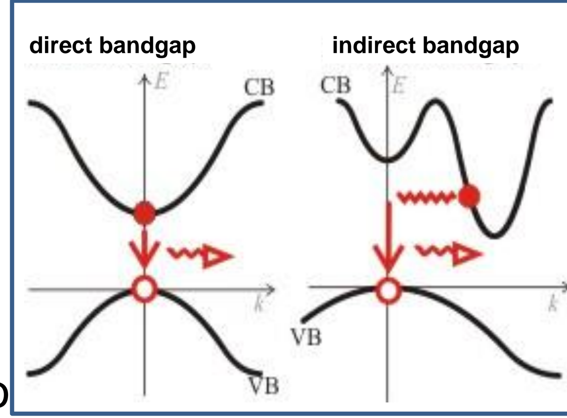

- Direct band gap materials are used to make photonic devices such as LEDs, semiconductor lasers.
- The band structure of Ge is a strong function of strain and alloy composition.
- Ge becomes a direct band gap material at ~2% tensile strain. [1]
- Relaxed $Ge_{1-y}Sn_y$ alloys become direct at ~6-9% Sn. [2,3,4]

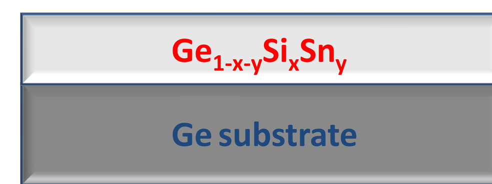

- $Ge_{1-x-y}Si_xSn_y$ → two compositional degrees of freedom allow decoupling of the lattice constant and electronic structure.
- **Pseudomorphically grown $Ge_{1-x-y}Si_xSn_y$** on Ge has low defect density and no dislocations.
- Band gap engineering of Ge by controlling strain and alloying with Si and Sn has attracted great interest.

Theory and Model

Lattice parameter of relaxed $Ge_{1-x-y}Si_xSn_y$ ternary alloys:

a_{Sn} = 6.489 Å > a_{Ge} = 5.657 Å > a_{Si} = 5.453 Å

$$a^{rel}_{Ge_{1-x-y}Si_xSn_y} = x a_{Si} + y a_{Sn} + (1-x-y) a_{Ge} + b_{GeSi}\, x(1-x-y)$$

Pseudomorphic $Ge_{1-x-y}Si_xSn_y$ on Ge:

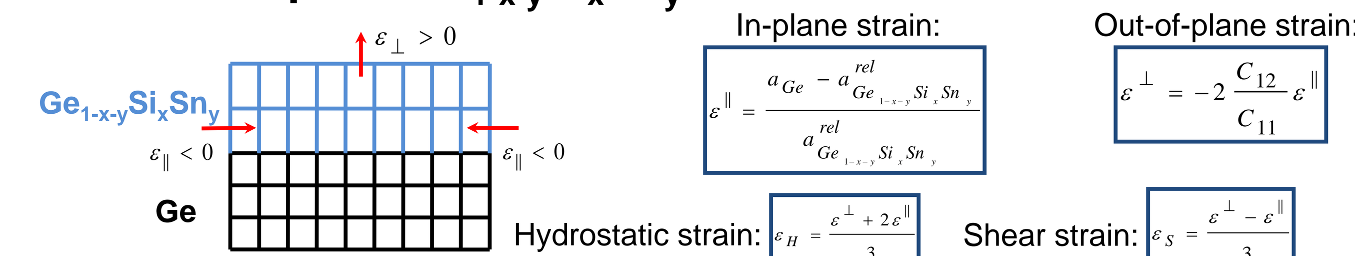

In-plane strain:

$$\varepsilon^{\parallel} = \frac{a_{Ge} - a^{rel}_{Ge_{1-x-y}Si_xSn_y}}{a^{rel}_{Ge_{1-x-y}Si_xSn_y}}$$

Out-of-plane strain:

$$\varepsilon^{\perp} = -2\frac{C_{12}}{C_{11}}\varepsilon^{\parallel}$$

Hydrostatic strain: $\varepsilon_H = \frac{\varepsilon^{\perp} + 2\varepsilon^{\parallel}}{3}$ Shear strain: $\varepsilon_S = \frac{\varepsilon^{\perp} - \varepsilon^{\parallel}}{3}$

Continuum elasticity and deformation potential theory: [5,6,7]

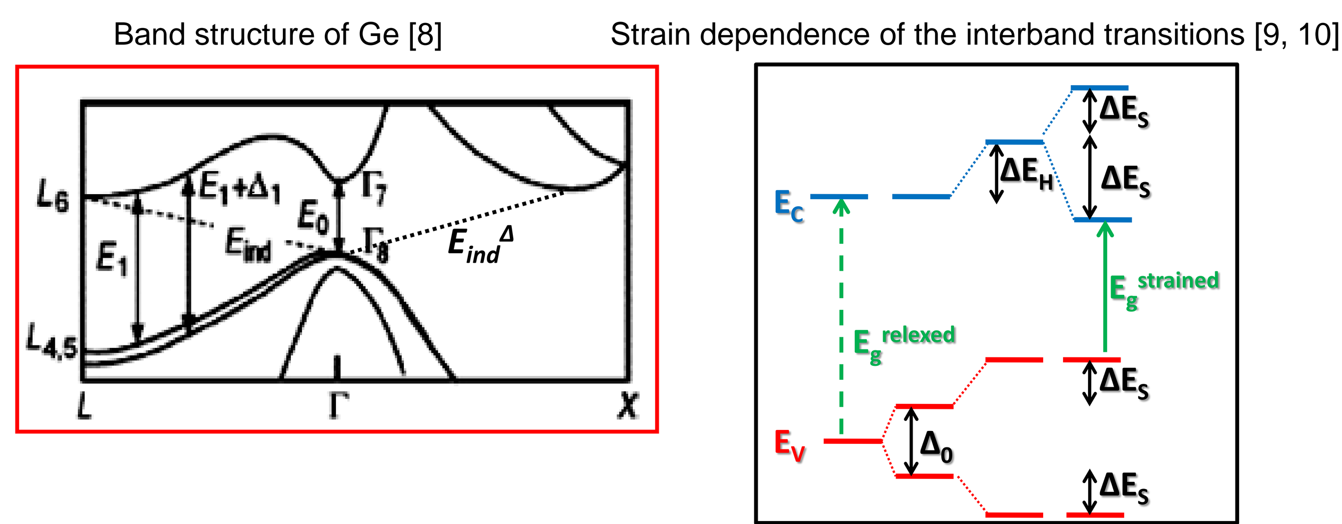

Effects of strain and alloying on Ge dielectric function

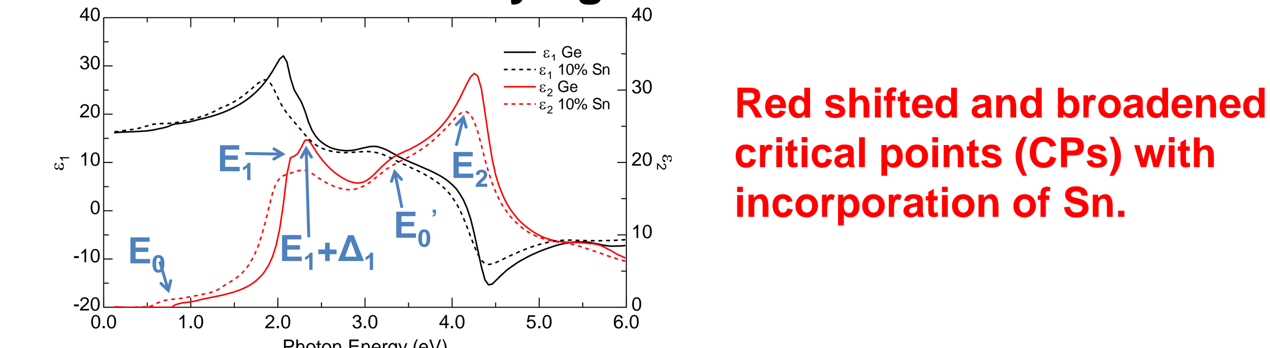

Figure 1. Real (ε_1) and imaginary (ε_2) parts of the dielectric function of Ge (solid) and pseudomorphic $Ge_{90}Sn_{10}$ on Ge (dashed).

Red shifted and broadened critical points (CPs) with incorporation of Sn.

Pseudomorphic $Ge_{1-x-y}Si_xSn_y$ on Ge

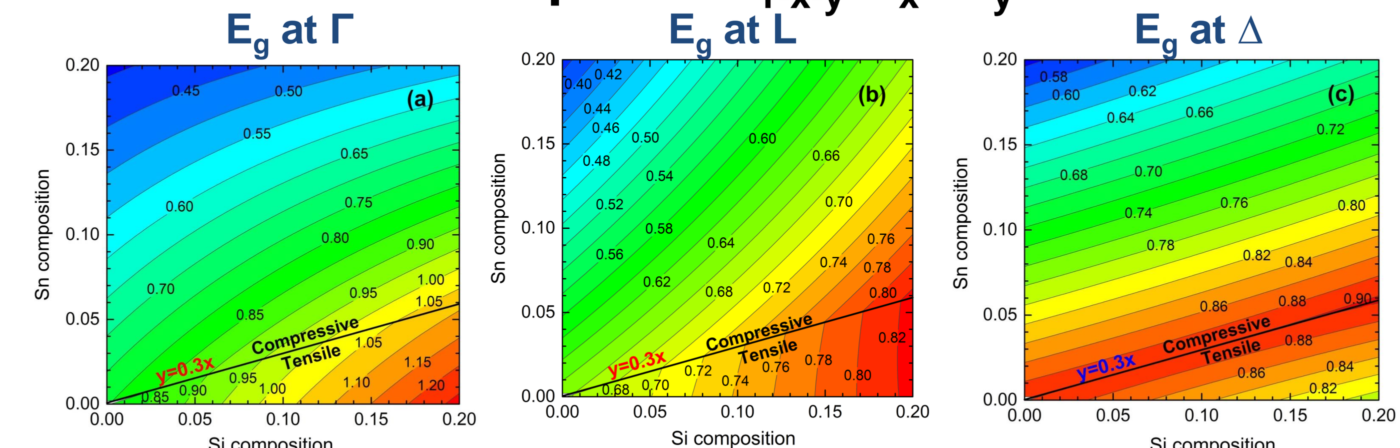

Figure 2. Band structure maps (energy in eV versus composition) of pseudomorphic $Ge_{1-x-y}Si_xSn_y$ alloys on Ge for band gaps at the (a) Γ, (b) L, and (c) Δ conduction band minima.

Direct-indirect transition of pseudomorphic $Ge_{1-x-y}Si_xSn_y$

Compositional dependence of the lowest band gap of pseudomorphic $Ge_{1-x-y}Si_xSn_y$ on different substrates:

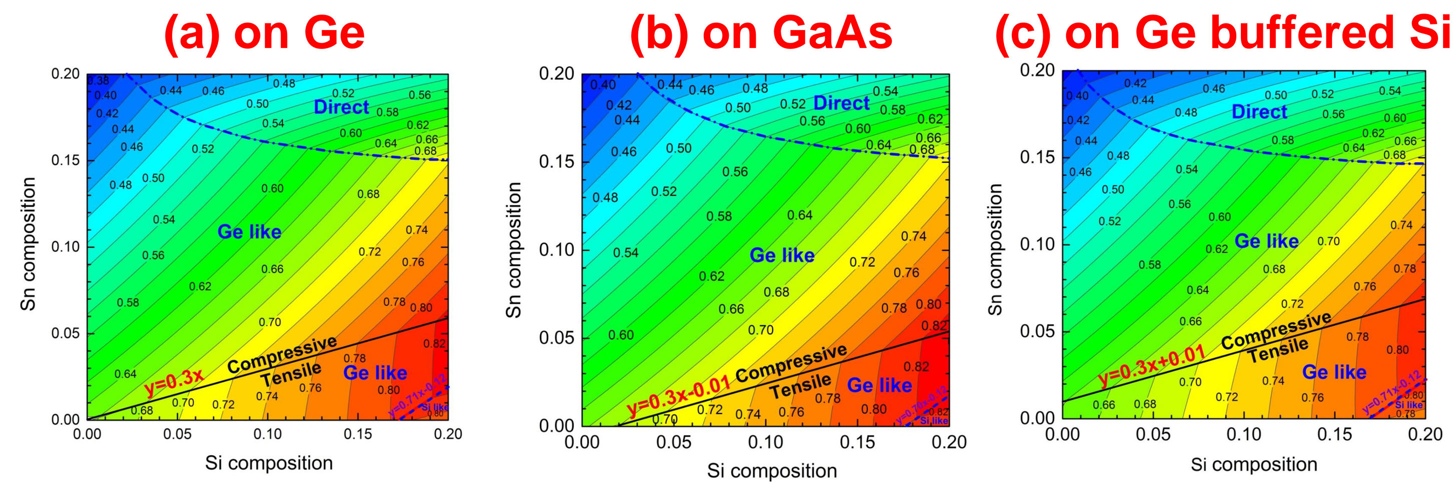

Figure 3. Compositional dependence of the lowest band gap (either direct or indirect) of pseudomorphic $Ge_{1-x-y}Si_xSn_y$ alloys on (a) Ge, (b) GaAs, and (c) a thick Ge buffer grown fully relaxed at 770 K on Si.

Direct-indirect transition of pseudomorphic $Ge_{1-y}Sn_y$ on Ge

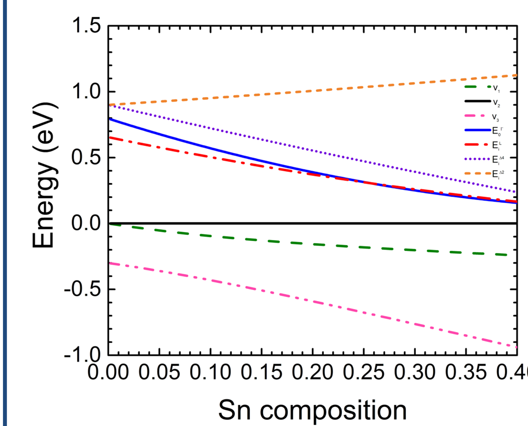

Figure 4. Energies of the three top valence bands at the Γ point (v_1, v_2, v_3), the conduction band minimum at the Γ point (E_c^{Γ}), at the L point (E_c^{L}), and at the Δ (E_c^{Δ}).

$E_c^{\Gamma} > E_c^{L}$ for practically approachable Sn

No direct gap possible

Pseudomorphic $Ge_{1-y}Sn_y$ on Ge

Sample preparation (at University of Delaware)

- **Molecular beam epitaxy (MBE)** [11]
- **EPI 620 MBE system with a base pressure of 1.3x10^-8 Pa**
- **Growth temperature 150° C -250° C, growth rate 0.6 – 0.7 nm/min**

Spectroscopic Ellipsometry (UV-Visible, FTIR)

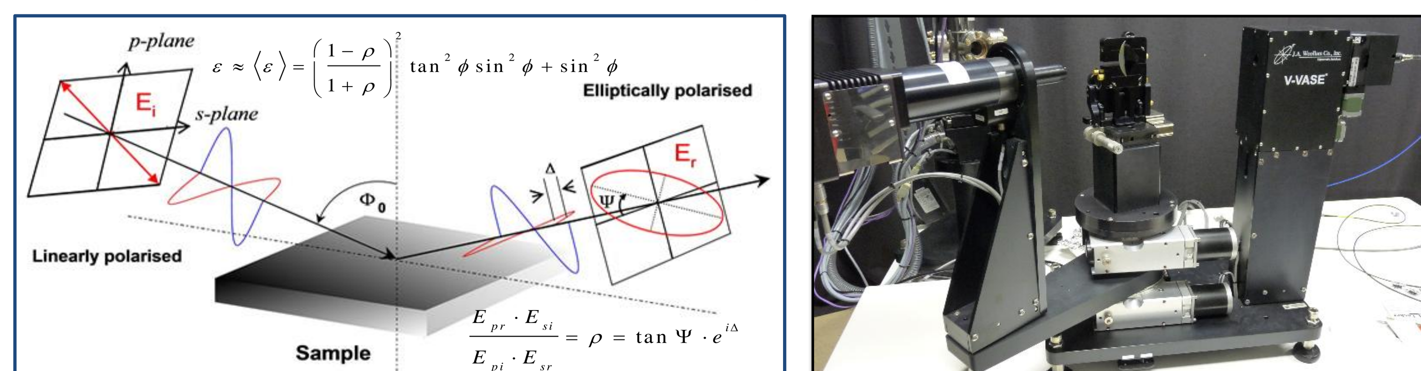

Figure 5. (Left) Schematic Overview of the measurement principle of the spectroscopic ellipsometry. (Right) A picture of the V-VASE.

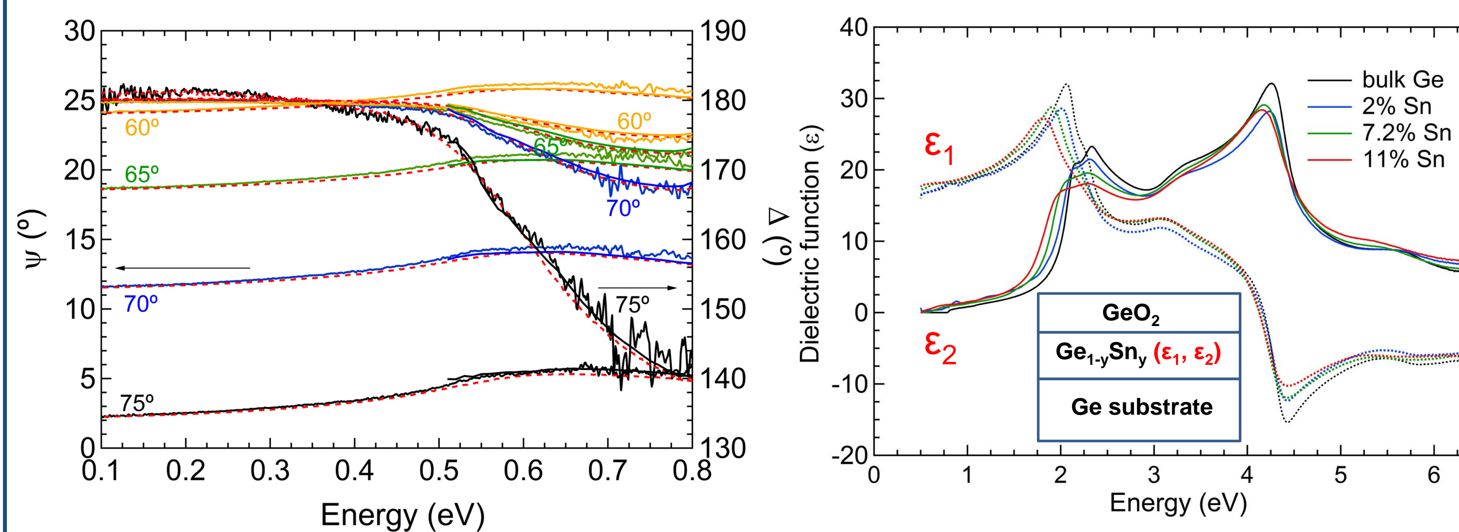

Figure 6. (Left) Experimental data (solid) and model (dashed) of the ellipsometric angles ψ and Δ for pseudomorphic $Ge_{0.89}Sn_{0.11}$ on Ge versus photon energy in the infrared region obtained by merging the data from FTIR and UV-Visible ellipsometers. (Right) Real ε_1 and imaginary parts ε_2 of the complex dielectric function of pseudomorphic $Ge_{1-y}Sn_y$ on Ge versus photon energy determined from ellipsometry, assuming a multi layer model $GeO_2/Ge_{1-y}Sn_y/Ge$.

- E_1 and $E_1+\Delta_1$ → 2D critical points: $\varepsilon = C - A \ln(E_g - \omega - i\Gamma)\, e^{i\Phi}$
- E_0 → 3D critical points: $\varepsilon \sim C - A(\omega - E_g + i\Gamma)^{1/2}\, e^{i\Phi}$
- Analysis of $d^2\varepsilon/dE^2$ → CP parameters: E_g- energy, A- amplitude, Γ- broadening, Φ- excitonic phase angle [12,13]

High resolution X-ray diffraction, X-ray reflectivity and AFM

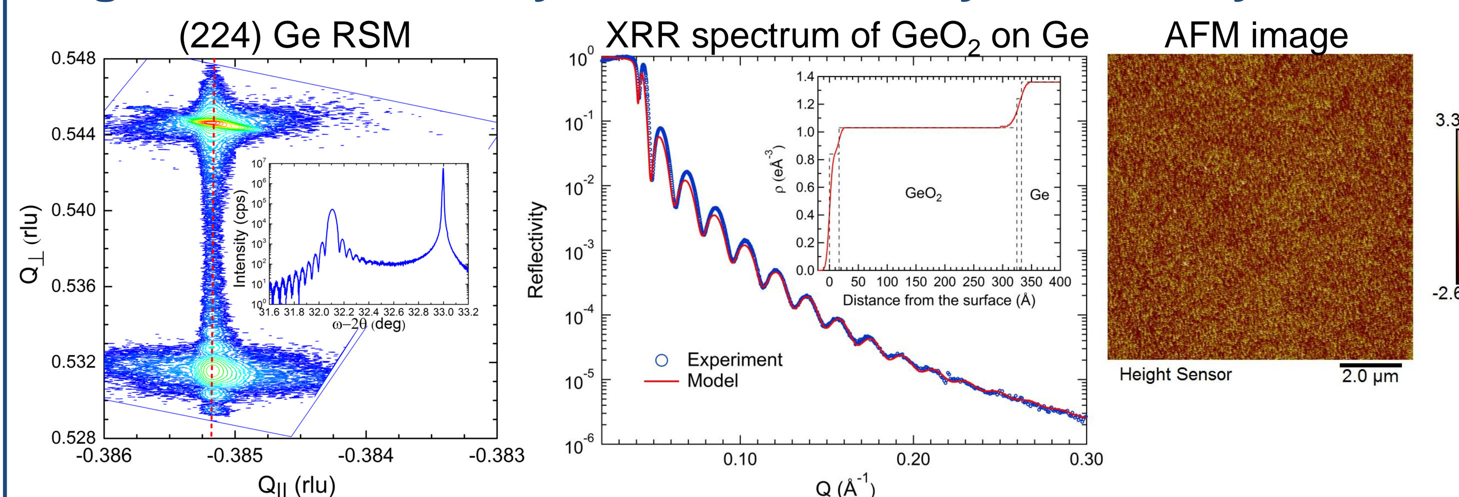

Figure 7. (Left) High-resolution X-ray diffraction (224) grazing exit reciprocal space maps of a $Ge_{0.094}Sn_{0.096}$ layer on Ge. Logarithmic intensity versus diffraction angle for the symmetric (004) ω-2θ X-ray reflection is shown in the inset. (Middle) X-ray reflectivity spectrum of a 33 nm thick GeO_2 on Ge. Electron density profile obtained from the model for the same sample is shown in the inset. (Right) Atomic force microscopy image of the $Ge_{0.094}Sn_{0.096}$ surface showing an RMS roughness of 1.6 nm.

Results: Pseudomorphic $Ge_{1-y}Sn_y$ on Ge

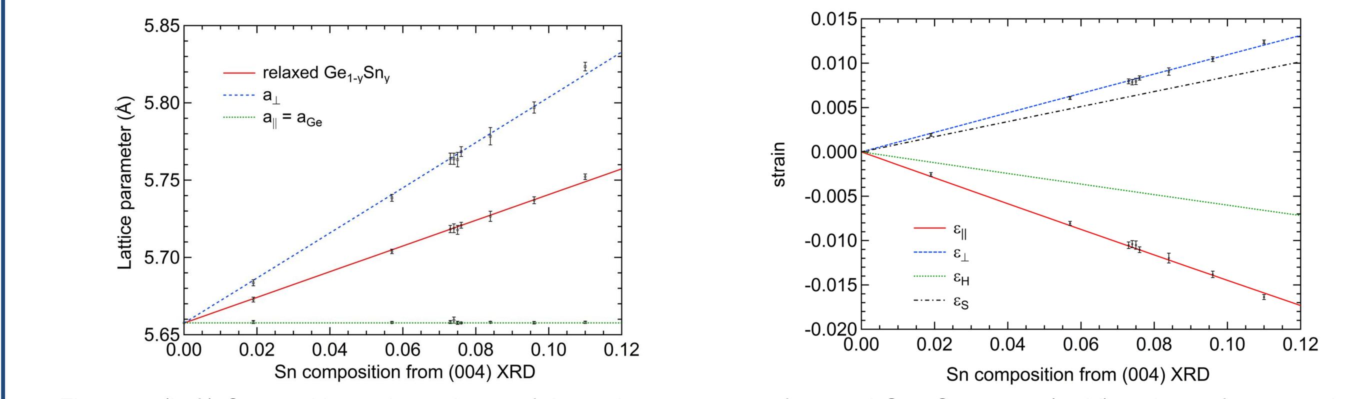

Figure 8. (Left) Compositional dependence of the lattice parameter of relaxed $Ge_{1-y}Sn_y$ alloys (solid) and out-of-plane lattice parameter $a_{\perp}$ of pseudomorphic $Ge_{1-y}Sn_y$ on Ge (dashed). (Right) Compositional dependence of the in-plane strain $\varepsilon_{\parallel}$, out-of-plane strain $\varepsilon_{\perp}$, hydrostatic strain ε_H, and shear strain ε_S for pseudomorphic $Ge_{1-y}Sn_y$ on Ge. Symbols show the values derived from X-ray diffraction data. Lines represent the calculated values using Vegard's law and elasticity theory.

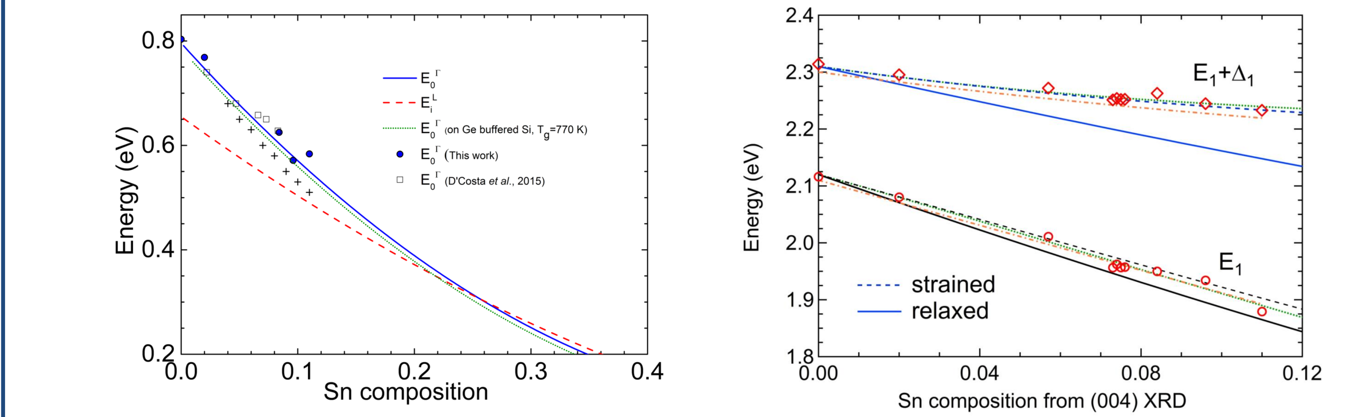

Figure 9. Compositional dependence of the (left) direct (E_c^{Γ}) and indirect (E_c^{L}) band gaps, and (right) E_1 and $E_1+\Delta_1$ band gaps of pseudomorphic $Ge_{1-y}Sn_y$ on Ge. Symbols show the experimental data obtained from spectroscopic ellipsometry. Lines are for the compositional dependence of the band gaps, calculated using deformation potential theory. [14, 15]

Results: Partially relaxed $Ge_{1-y}Sn_y$ on Ge (large y)

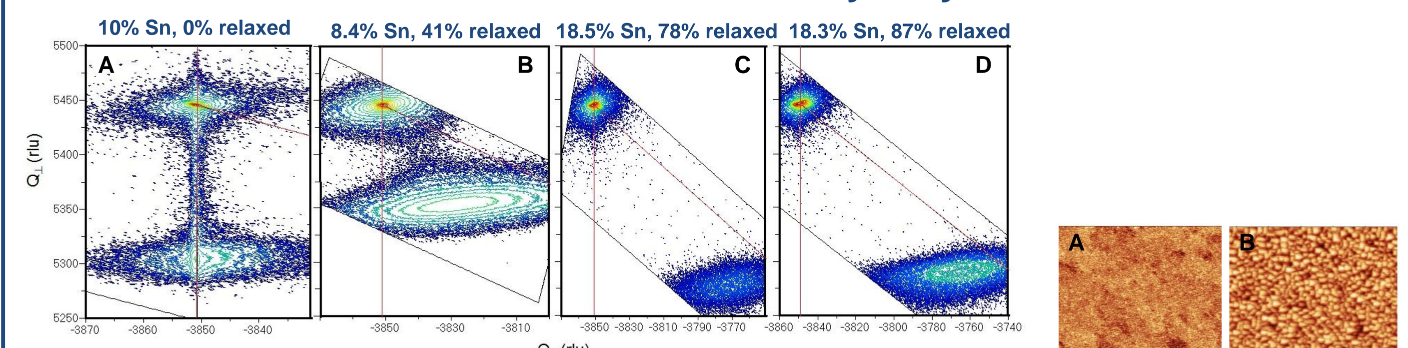

Figure 10. (224) grazing exit reciprocal space maps (RSMs) for partially relaxed $Ge_{1-y}Sn_y$ on Ge samples. The vertical line represents 100% compressive strain (pseudomorphic). The diagonal line represents complete relaxation.

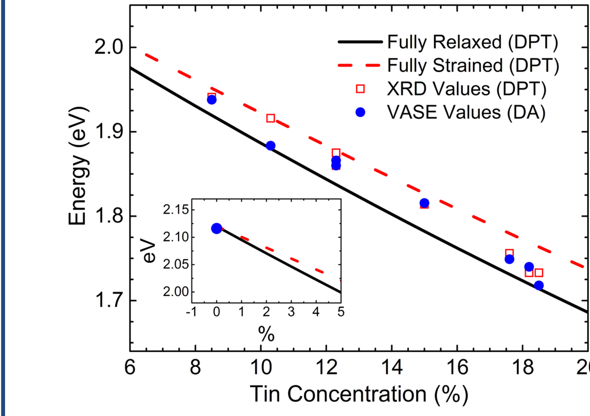

Figure 11. AFM images of the samples. The RMS roughness was 0.69, 3.77, 0.71, and 1.0 nm for the samples A, B, C and D respectively. Images showed that the periodic roughness, caused by strain induced buckling, depended on the $Ge_{1-y}Sn_y$ thickness and relaxation. [11]

Figure 12. Compositional and strain dependence of the E_1 critical point for $Ge_{1-y}Sn_y$ on Ge. Solid line is fully relaxed and dashed line is pseudomorphically strained. Circles represent the measured E_1 from ellipsometry. Squares represent the calculated E_1 using deformation potential theory, taking into account the Sn content and degree of relaxation determined from X-ray diffraction. [11]

Conclusion

- Pseudomorphic $Ge_{1-x-y}Sn_y$ on Ge: Indirect –direct transition requires impossibly large Sn content, ~15-20%.
- Increasing the growth temperature of the Ge buffer layer reduces the compressive strain → reduces the x (Si) and y (Sn) for the indirect to direct crossover (not significantly).
- Deformation potential theory predicts no indirect to direct band gap crossover for pseudomorphic (fully strained) $Ge_{1-y}Sn_y$ alloys on Ge for Sn < 25%.
- Experimental results obtained from ellipsometry for $Ge_{1-y}Sn_y$ alloys are in good agreement with the prediction.
- Strain relaxation is critical for the indirect-direct transition.

Acknowledgement

This work was supported by the Air Force Office of Scientific Research (FA9550-13-1-00222) and by the Army Research Office (W911NF-14-1-0072). Support during 2016 was provided by the National Science Foundation (DMR-1505172). FTIR measurements were performed by Stefan Schoeche and James Hilfiker at J.A. Woollam Co., Inc., Lincoln, NE.

References

1. M. El Kurdi, G. Fishman, S. Sauvage, and P. Boucaud, J. Appl. Phys. **107**, 013710 (2010).
2. G. He and H.A. Atwater, Phys. Rev. Lett. **79**, 1937 (1997).
3. J. Mathews, R.T. Beeler, J. Tolle, C. Xu, R. Roucka, J. Kouvetakis, and J.Menendez, Appl. Phys. Lett. **97**, 221912 (2010).
4. C. Eckhardt, K. Hummer, and G. Kresse, Phys. Rev. B **89**, 165201 (2014).
5. H.J. Osten, J. Appl. Phys. **84**, 2716 (1998).
6. M. Chandrasekhar and F.H. Pollak, Phys. Rev. B **15**, 2127 (1977).
7. J. Menendez and J. Kouvetakis, Appl. Phys. Lett. **85**, 1175 (2004).
8. M.R. Bauer, J. Tolle, C. Bungay, A.V.G. Chizmeshya, D.J. Smith, J. Menendez, and J. Kouvetakis, Solid State Commun. **127,** 355 (2003).
9. V.R. D'Costa, W. Wang, Q. Zhou, E.S. Tok, and Y.C. Yeo, Appl. Phys. Lett. **104**, 022111 (2014).
10. A. Attiaoui and O. Moutanabbir, J. Appl. Phys. **116**, 063712 (2014).
11. R. Hickey, N. Fernando, S. Zollner, J. Hart, R. Hazbun, and J. Kolodzey, J. Vac. Sci. Technol. B **35**, 021205 (2017).
12. L. Vina, S. Logothetidis, and M. Cardona, Phys. Rev. B **30**, 1979 (1984).
13. V. R. D'Costa, W. Wang, and Y. Yeo, J. Appl. Phys. **120**, 063104 (2016).
14. M. Medikonda, G.R. Muthinti, R. Vasic, T.N. Adam, A. Reznicek, M. Wormington, G. Malladi, Y. Kim, Y.C. Huang, and A.C. Diebold, J. Vac. Sci. Technol. B **32**, 061805 (2014).
15. V.R. D'Costa, W. Wang, Q. Zhou, T.K. Chan, T. Osipowicz, E.S. Tok, and Y.C. Yeo, J. Appl. Phys. **116**, 053520 (2014).